

First observation and measurement of the ^{198}Hg bosonic transition in an optical lattice clock

Clara Zyskind, Thomas Lauprêtre, Haosen Shang, Benjamin

Pointard, Rodolphe Le Targat, Jérôme Lodewyck, and Sébastien Bize

LTE (LNE-OP), Observatoire de Paris-PSL, CNRS, Sorbonne Université, Université de Lille, LNE

(Dated: December 5, 2025)

We report the first observation of the magnetic-field-induced $(5d^{10}6s^2)^1\text{S}_0$ – $(5d^{10}6s6p)^3\text{P}_0$ transition in a bosonic isotope of mercury, ^{198}Hg , realized in an optical lattice clock. We characterize this new isotope, determining key features such as the quadratic Zeeman shift, the probe light shift, and the magic frequency. We also report a first comparison between the ^{198}Hg optical lattice clock and ^{87}Sr . In this comparison, the ^{198}Hg clock has a relative frequency stability of $6 \times 10^{-16}/\sqrt{\tau/\text{s}}$ and a total relative systematic uncertainty of 6.9×10^{-16} . This comparison yields the first direct determination of the $^{198}\text{Hg}/^{87}\text{Sr}$ optical frequency ratio: $^{198}\text{Hg}/^{87}\text{Sr} = 2.629\,315\,734\,684\,118\,1$, with the same relative uncertainty.

Recent advances in optical frequency metrology, particularly the development of ultrastable lasers with fractional frequency instability lower than 10^{-16} [1–3], have enhanced the capability of optical clocks. Fully benefiting from such lasers requires the ability to probe the clock transition for duration exceeding 1 s, which is not accessible to all atomic species considered for optical clocks. Achieving the highest stability and accuracy requires selecting atomic transitions with longer lifetimes, in addition to minimal sensitivity to external perturbations.

Among neutral atoms, mercury offers promising properties for optical lattice clocks. Its low sensitivity to thermal radiation and stray electric fields makes it significantly less affected by blackbody radiation than other species [4]. To date, only the $^1\text{S}_0$ – $^3\text{P}_0$ clock transition of fermionic ^{199}Hg has been studied in a lattice clock [4–7]. This transition is weakly allowed by hyperfine mixing, which governs the spontaneous emission rate from $^3\text{P}_0$ to $^1\text{S}_0$, setting the $^3\text{P}_0$ lifetime. In ^{199}Hg , the lifetime is short, ~ 1.5 s [8, 9], which may limit the advantages of next-generation ultrastable lasers [1, 2] that enable longer probing times and improved stability [10–12].

Using bosonic mercury isotopes circumvents this limitation. With zero nuclear spin, their $^1\text{S}_0$ – $^3\text{P}_0$ transition is strictly forbidden, so the $^3\text{P}_0$ state does not spontaneously decay. This transition can be weakly induced by applying a strong static magnetic field \mathbf{B} , as proposed in [13] and demonstrated in ^{88}Sr [14–16] and ^{174}Yb [17]. The magnetic field primarily mixes the $^3\text{P}_0$ and $^3\text{P}_1$ states (Fig. 1) via the magnetic-dipole coupling $\hbar\Omega_B = \langle ^3\text{P}_0 | \hat{\mu} \cdot \mathbf{B} | ^3\text{P}_1 \rangle$, with $\hat{\mu}$ the magnetic-dipole operator, perturbing $^3\text{P}_0$ with a small $^3\text{P}_1$ admixture. As a result, the otherwise forbidden $^1\text{S}_0$ – $^3\text{P}_0$ transition acquires a weak electric-dipole amplitude through the $^1\text{S}_0$ – $^3\text{P}_1$ coupling $\hbar\Omega_L = \langle ^1\text{S}_0 | \hat{\mathbf{d}} \cdot \mathbf{E} | ^3\text{P}_1 \rangle$, driven by an optical field of amplitude \mathbf{E} and frequency ω . Residual coupling to other states, such as $^1\text{P}_1$, also exists (Fig. 1). This magnetic-field-induced mixing allows tuning at will of the transition strength, enabling extended probe times to match the coherence time of the probe laser.

However, direct laser excitation of a bosonic mercury

clock transition has not yet been observed. Here, we report the first observation of the ^{198}Hg bosonic transition in an optical lattice clock and the first measurement of the $^{198}\text{Hg}/^{87}\text{Sr}$ optical frequency ratio, enabled by several key experimental advances and a challenging search for a narrow transition across a wide uncertainty range.

The setup for searching the bosonic clock transition builds on the existing experiment used for probing the ^{199}Hg fermionic isotope, as described in [7, 18–22].

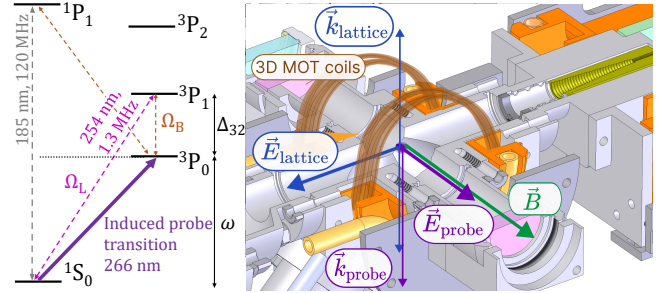


FIG. 1. (Left) The ^{198}Hg bosonic clock transition magnetic-field induced mixing scheme: The doubly forbidden $^1\text{S}_0$ – $^3\text{P}_0$ transition is enabled by a strong static magnetic field \mathbf{B} , coupling the $^3\text{P}_0$ and $^3\text{P}_1$ states via the matrix element Ω_B through magnetic dipole interaction (dotted orange lines). The cooling transition $^1\text{S}_0$ – $^3\text{P}_1$ with its electric dipole coupling Ω_L is indicated by the dotted pink line. (Right) Probing configuration for ^{198}Hg : The probe beam polarization is aligned with the magnetic field from 3D MOT coils. The vertical lattice is polarized perpendicular to the probe beam.

First, a well-controlled and sufficiently strong magnetic field is required to induce the mixing. For this, we generate a pulsed magnetic field by using the 3D MOT coils and switching electronics to rapidly reverse the current in one of the coils during interrogation, following the approach used in [17]. A maximum field of $B = 18.6$ mT can be reached with 12 A current, with rise/fall times as fast as $3/2.8$ ms to minimize unwanted dead times. Three additional pairs of coils compensate residual background magnetic fields. Their current is set by minimizing the Zeeman splitting of the ^{199}Hg clock transition.

Next, we extended our ultrastable light generation to provide a sufficiently broad continuous tuning range to reach the bosonic isotope. We implemented a setup with an intermediate laser [23], which is offset phase-locked to the ultrastable light. This offers greater flexibility than the original design [18, 19] and enables ultrastable probing at 266 nm across all mercury isotopes, rather than being limited to ^{199}Hg . We also ensured that spectral purity was maintained at the present 4×10^{-16} flicker frequency noise level for the ultrastable light [24] and that the system remains compatible with future improvements well beyond this stability.

In order to facilitate the search for the transition, achieving the highest possible coupling in our setup was critical. As it scales with intensity, we first enhanced our deep-UV probing light to a maximum of 400 μW at 266 nm. By then reducing the probe waist to 63.5 μm , intensities as high as $I_0 = 6.3 \text{ W/cm}^2$ could be reached at the center of the beam. With the probe polarization aligned to the applied magnetic field B (Fig. 1), the estimated Rabi frequency is $\Omega_{12} = \frac{\Omega_r \Omega_B}{\Delta_{32}} = \alpha \sqrt{IB}$ [13], giving $\Omega_{12}/2\pi \simeq 75 \text{ Hz}$, where α is the magnetic-field-induced coupling coefficient and Δ_{32} the angular frequency detuning between $^3\text{P}_1$ and $^3\text{P}_0$.

With such a weak coupling, a frequency range for the search that is too large becomes prohibitive. The best-predicted bosonic mercury clock transition corresponded to ^{198}Hg [25, 26], motivating our focus on this specific isotope. As ^{198}Hg atoms are trapped in the optical lattice, another potential challenge was the lack of knowledge on the exact lattice magic frequency [27]. Indeed, a largely detuned lattice frequency broadens and degrades the contrast of the clock resonance. We set the lattice frequency to the magic frequency of the fermionic ^{199}Hg , as calculations and experimental tests with this isotope showed that contrast would be preserved over the expected lattice detuning range. The lattice trap depth was set to $92.4 E_r$, with the recoil energy $E_r = h \times 7.57 \text{ kHz}$.

When trapping ^{198}Hg , we measured a MOT loading time constant of 1.2 s and a lattice lifetime of 200 ms, both comparable to those of fermionic ^{199}Hg .

Once the experimental setup ready, we conducted a thorough exploration over the predicted frequency range for the ^{198}Hg bosonic transition [25], scanning a total range of 25 MHz by 120 Hz steps (Fig. 2, top). This meticulous search led to the first successful observation of the bosonic transition. Its frequency lies slightly beyond the $\pm 1\sigma$ uncertainty of [25] and beyond $\pm 2\sigma$ of [26].

Once the transition found, we measured an experimental Rabi frequency to actually be $\Omega_{12}/2\pi = 45 \text{ Hz}$. Optimizing parameters (magnetic field reduced by a factor 10 and a lower probing power) allowed a probing time of 200 ms giving spectra with a 4 Hz full width at half maximum (Fig. 2, bottom). Operating a clock sequence with such parameters and analyzing the noise of frequency corrections, we estimate that the clock stability surpasses by a factor ~ 2 the stability previously achieved with the fermionic isotope [22]. From comparisons against local

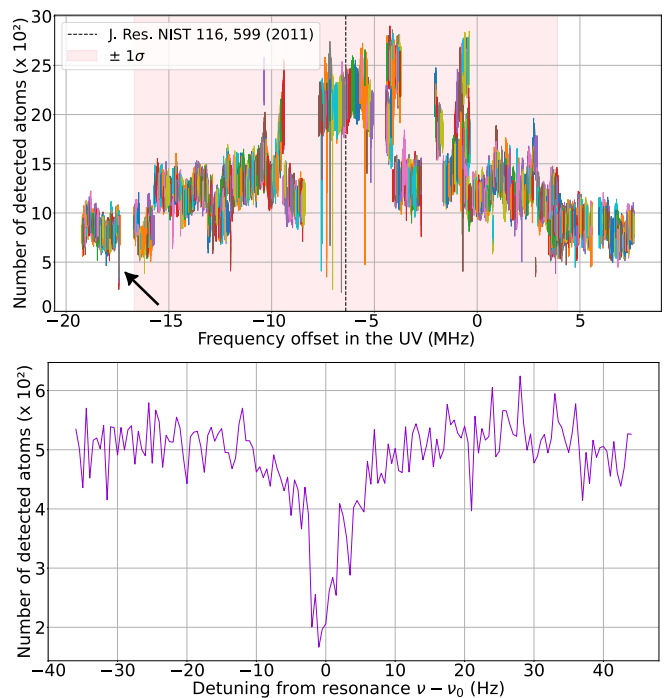


FIG. 2. (Top) All spectra acquired for the search of the ^{198}Hg transition in the optical lattice. Each color corresponds to a scan covering a specific range of 100 kHz by steps of 120 Hz. In total, more than 25 MHz were scanned before successfully identifying the transition (black arrow). (Bottom) Narrowest ^{198}Hg spectroscopy obtained, after optimization: for 200 ms probe time, the full width at half maximum is 4 Hz.

Sr clocks, we infer stabilities of $\sim 6 \times 10^{-16}/\sqrt{\tau/s}$ for the ^{198}Hg bosonic clock.

Having identified the new transition, we measured key systematic effects to characterize its properties. First, a high magnetic field is required to couple the transition. Although there is no linear Zeeman shift due to zero nuclear spin, a significant quadratic Zeeman shift (QZS) is expected and observed, necessitating accurate measurement. The QZS is given by $\Delta_B = \beta B^2$, with $\beta/2\pi$ in Hz/T^2 . We measured β using an intertwined differential method: two alternating configurations, differing only in the applied magnetic field, produce different QZS from which we extract a differential shift value.

To achieve the required accuracy in determining β , we carefully characterized the current source generating the applied magnetic field. Nonlinearities in current control were accounted for, transients from rapid switching were mitigated via optimized timing, and long-term reproducibility was verified through current monitoring (yielding a 10 μA uncertainty). In Fig. 3, we show the measured QZS coefficient and its statistical uncertainty (blue points and error bars) against the difference of squared currents, where $\beta_A/2\pi$ is expressed in units of Hz/A^2 . Most data points were taken during an initial round, supplemented by 3 points measured 20 months later. Their average gives the mean value and uncertainty. However, residual inconsistencies in the QZS data

were observed in this initial dataset, with the two most inconsistent points differing by 6.3σ . To obtain a reasonable uncertainty despite the unknown origin of these fluctuations, we modeled the dispersion by adding uncorrelated noise and adjusted the error bars accordingly to reflect the total noise [28]. The updated results, shown in Fig. 3 (orange error bars), give a QZS coefficient of $\beta_A/2\pi = -6.9237 \pm 0.0043$ Hz/A². For the lowest value of the current we used so far (1.13 A), the corresponding fractional uncertainty on the QZS correction is 4×10^{-18} .

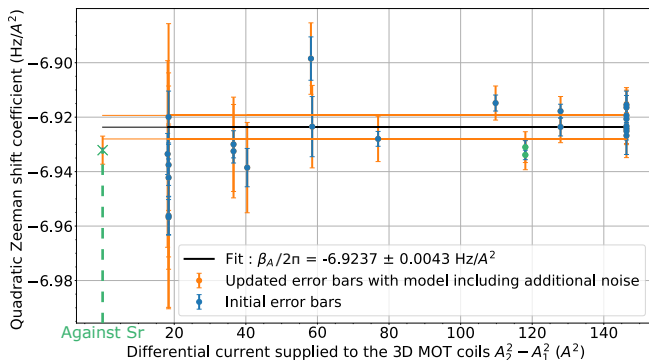


FIG. 3. Measurement of the quadratic Zeeman shift coefficient $\beta_A/2\pi$ with initial error bars (blue) and error bars incorporating a model with additional uncorrelated noise (orange). See text for more details. Blue and green dots represent differential measurements from Mar.-Apr. 2024 and Sep. 2025, respectively. The cross symbol is a value deduced from 3 direct measurements against a Sr clock at currents of 1.1 A, 3.6 A and 10.9 A [29]. The black line represents the estimated coefficient returned by the fit of the measurement values with the modeled error bars. The orange lines represents our final uncertainty range ($\pm 1\sigma$), where σ is defined here as the smallest modeled error bar.

Uncertainties arising from magnetic field fluctuations and residual magnetic field also need to be addressed. With a magnetic field probe, we detect fluctuations of 1 μ T. The residual field is minimized to less than 1.5 μ T. These fluctuations were estimated to have a negligible impact on the measurement of β . In Table III, we give the QZS correction and uncertainties for 3.6 A, the highest value applied to our frequency ratio determination.

Lastly, to compare the QZS coefficient with its theoretical value (Table I), it was converted to magnetic field units using a geometric factor of 1.527 ± 0.04 mT per ampere of current flowing through the 3D MOT coils.

Another essential parameter of the bosonic isotope probing scheme is the magnetic-field-induced coupling coefficient α , describing the coupling between ground and excited states via the external applied magnetic field. To determine α , we measured Rabi frequencies at constant probe intensity I while varying B , yielding a linear relationship whose slope gives α . We accounted for experimental factors affecting the measured Rabi frequencies to ensure accuracy. The 63.5 μ m probe waist is comparable to the atomic distribution size, causing the atoms to experience an inhomogeneous probe beam intensity and

hence different Rabi frequencies, leading to damped Rabi oscillations. We used a simplified model that averages the Rabi oscillation over the transverse atomic distribution to estimate a factor linking the first maximum of the measured Rabi flopping curve to the Rabi half-period in the ideal case of an atom at the center of the probe beam, thereby seeing the peak intensity. We find a correction factor of 1.3, in line with strong inhomogeneity. The resulting value of α is given in Table I.

Another crucial parameter to measure for an optical lattice clock is the magic frequency, the non-perturbing lattice frequency at which the light shift is canceled at any trapping depth [27]. The magic frequency is an intrinsic atomic property that varies between species and isotopes, therefore its precise value must be determined for the ¹⁹⁸Hg bosonic isotope. To measure the ¹⁹⁸Hg magic lattice frequency, we performed differential measurements between two different lattice depths: 92.4 E_r and 79.3 E_r . Fig. 4 shows the differential clock shift as a function of the lattice frequency ν_L . The lattice frequency was precisely known and stabilized using an optical frequency comb with the setup described in [30].

Given our limited trapping depth range and our frequency resolution, a linear approximation of the lattice light shift is justified to analyze our measurements. In this approximation, the lattice light shift (LLS) is proportional to both the lattice depth (in units of recoil energy E_r) and the detuning of the lattice laser from the magic frequency. For a configuration with lattice depth U_x ($x = 1, 2$), the resulting fractional frequency shift is $y_x = \eta(\nu_L - \nu_L^m)U_x$ where η is the experimental slope of the linear LLS. The magic frequency ν_L^m is found at the detuning where the differential lattice light shift is equal to zero. From this analysis, we extract a magic frequency of $\nu_L^m = 826\,855\,228 \pm 28$ MHz, as shown in Fig. 4. We note that the corresponding uncertainty (Table III) is set by limitations of our setting and not by any fundamental limitation associated to ¹⁹⁸Hg.

We also studied the cold collisional shift (CCS) which arises from interactions between cold atoms and depends on the atomic density, closely linked to the atom number during interrogation N_{atoms} . To estimate it, we compute the integral of the decay of the atom number inside the lattice over the probe pulse timing, based on the number of atoms detected later in the detection. The maximum effective atom number during interrogation is $\sim 10^3$, corresponding approximately to one atom per lattice site at the trap center. Atom number was varied by turning on the MOT beams later in the sequence while keeping other key parameters unchanged, such as cycle time and MOT loading time, ensuring a method that is as differential as possible. For differential atom numbers up to 550, we observed an absence of shift well within our typical resolution of 10^{-16} . In these conditions, it is reasonable to analyze these measurements under the simplifying assumption that the fractional CCS is proportional to N_{atoms} . Doing so, the CCS found is $(-3 \pm 14) \times 10^{-20} \times N_{\text{atoms}}$.

The probe light itself induces an AC Stark shift of the

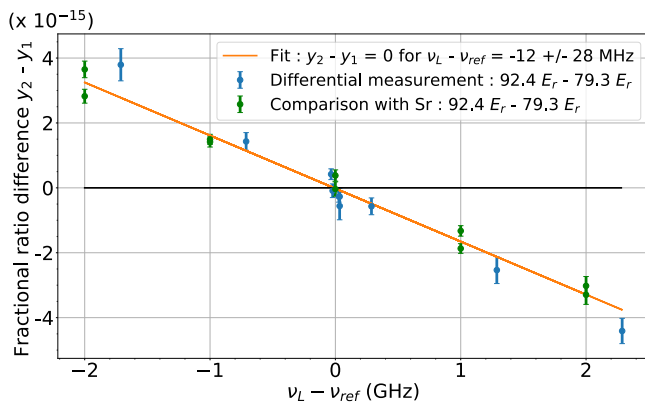


FIG. 4. Magic frequency determination from two series of differential measurements: one with the Hg clock alone and one assisted by a Sr clock [31, 32] to improve stability. The reference used for the lattice frequency is $\nu_{\text{ref}} = 826\,855\,240$ MHz. The linear fit (orange) returns the value of the magic frequency $\nu_L^m = 826\,855\,228 \pm 28$ MHz for ^{198}Hg . It also gives the experimental slope of $\eta = (-1.41 \pm 0.04) \times 10^{-4}$ Hz/ E_r /MHz. Both are used to estimate the lattice light shift correction and its uncertainty.

clock levels resulting in a shift of the transition frequency proportional to the probe intensity $\Delta_L(\text{rad/s}) = \kappa I$. To determine κ , we measured frequency shifts against Sr clocks [31, 32] while varying the probe power P . We made pairs of measurements at P and $P/2$ while keeping the probe duration, the magnetic field and all other parameters of the sequence the same. This came at the cost of using a non-optimal probe pulse in both cases, one stronger and one weaker than the optimum. We also made measurements with optimal pulses. Overall we explored a power range from 1 to 500 μW , corresponding to a central beam intensity I_0 experienced by the atoms ranging from 15 mW/cm^2 to 7.9 W/cm^2 .

Once again, the probe intensity exhibits significant inhomogeneities across the atomic sample that must be taken into account. To do so, we expand the simple model used for extracting α to include the transverse distribution of detunings caused by the probe light shift. For optimal pulses, the model shows that these inhomogeneities reduce the effective clock shift to about $0.76 \times \kappa I_0$. For $P-P/2$ measurements, the predicted slope is smaller by an additional factor of 0.9, and their linear extrapolation to $P = 0$ retains a bias of ~ 0.06 times the shift at P . Experimentally, we measure slopes of 33 $\text{mHz}/\mu\text{W}$ for optimal pulses with P in the 10–100 μW range. For the $P-P/2$ method, we obtain slopes from 11 to 29 $\text{mHz}/\mu\text{W}$ for P in the 50–500 μW range, with a mean of 22 $\text{mHz}/\mu\text{W}$. This is not fully consistent with the predicted ratio of slopes between the two methods. We further consider that the beam shape could significantly deviate from a Gaussian profile and that its alignment with the atomic sample may be imperfect or fluctuate over time. As a result, 20% is a reasonable relative uncertainty for our determination of κ given in Table I, which is derived from measurements with the optimal pulses.

TABLE I. Theoretical and experimental (this work) values along with their uncertainties for the coupling coefficient, the QZS coefficient, and the probe light shift coefficient. We note that for κ , due to the simplified model, we do not expect an agreement between the theoretical and experimental values.

	$\frac{\alpha/2\pi}{\text{Hz}}$ $\text{T}\sqrt{\text{mW}/\text{cm}^2}$	$\frac{\beta/2\pi}{\text{MHz}}$ T^2	$\frac{\kappa/2\pi}{\text{mHz}}$ mW/cm^2
Basic theory	54	-2.465	0.38
Experiments	45 ± 9	-2.969 ± 0.16	2.74 ± 0.55

We now aim to determine the factor of merit ξ for the induced mixing scheme, as defined in [13]. It characterizes the relationship between the coupling strength, which we seek to maximize, to the resulting field-induced shifts, which are undesirable. Specifically, the Rabi angular frequency can be expressed in terms of the probe light shift Δ_L and the quadratic Zeeman shift Δ_B as $\Omega_{12} = \alpha\sqrt{|\frac{\Delta_L}{\kappa} \frac{\Delta_B}{\beta}|} = \xi\sqrt{|\Delta_L \Delta_B|}$, where $\xi = \alpha/\sqrt{|\kappa\beta|}$ represents in other terms the effective excitation strength relative to the induced shifts. Table I lists the experimentally determined coefficients α , β and κ .

Table I also gives theoretical values that we computed taking into account the dominant coupling of $^3\text{P}_0$ to $^3\text{P}_1$, following [13], and adding the effect of $^3\text{P}_0$ to $^1\text{P}_1$. For the induced coupling α , we find that $^1\text{P}_1$ accounts for about 10% of the total effect. For the QZS coefficient β , the influence of $^1\text{P}_1$ is found negligible (about 0.1%). Due to the large experimental uncertainty in α , mainly arising from probe beam inhomogeneities, we retain the theoretical value of α to estimate ξ . On the contrary, for κ , we retain our experimental value because we know that the simplified model cannot accurately account for the polarizabilities of the clock states $^1\text{S}_0$ and $^3\text{P}_0$ and thereby not capture the probe light shift. With this approach, we obtain our best estimate of the factor of merit ξ , given in Table II, for the bosonic transition in Hg. It stands as the most favorable species, together with Yb, among several other considered species.

TABLE II. Factor of merit for several bosonic species considered for optical lattice clocks [13], including ^{198}Hg (this work).

	^{198}Hg	Sr	Yb	Ca	Mg
ξ	0.60	0.30	0.60	0.28	0.28

We operated the bosonic mercury lattice clock in two comparison campaigns against the local strontium clocks: a preliminary run in Jun. 2024 and a second after major operational optimization in Sep. 2025. In total, we accumulated about 40 hours of data. The systematic uncertainty budget is shown in Table III. The black-body radiation values rely on theoretical polarizabilities given in [4]. Background gas collision values rely on [33] and its practical implementation [34], applied to Hg [23]. The ^{87}Sr counterparts have negligible un-

TABLE III. Typical systematic effect corrections and uncertainties of the ^{198}Hg clock during the campaign for determining the $^{198}\text{Hg}/^{87}\text{Sr}$ optical frequency ratio. The QZS is given for a current of 3.6 A (field ~ 5.5 mT), and the probe light shift for a power of 100 μW ($I_0 \sim 1.6$ W/cm 2). During the campaign, data were acquired at these values or lower.

Effect	Correction ($\times 10^{-17}$)	Uncertainty ($\times 10^{-17}$)
Quadratic Zeeman effect	7868.7	4.9
Magnetic field fluctuations	0	2.9
Residual magnetic field	0	4.3
Cold collisional shift	4.1	17.3
Linear lattice light shift	0	32.3
Nonlinear lattice light shift	2.1	2.1
Blackbody radiation	14.6	1.5
Background gas collisions	3.0	3.0
Probe light shift	-291.8	58.4
Total	7600.6	69.4

certainties of 4.6×10^{-17} . We obtain a frequency ratio of $^{198}\text{Hg}/^{87}\text{Sr} = 2.629\,315\,734\,684\,118\,1$ with a fractional uncertainty of 6.9×10^{-16} . From this measured ratio and the CCTF 2021 recommended frequency and recommended uncertainty for ^{87}Sr [35], we derive the frequency of the bosonic ^{198}Hg clock transition:

$$\nu_{^{198}\text{Hg}} = 1\,128\,575\,945\,288\,666.3 \pm 0.78 \text{ Hz.}$$

The probe light shift dominates the uncertainty budget (Table III), mainly due to probe beam inhomogeneities and the difficulty of accurately controlling the probe intensity. This uncertainty could be further reduced using a hyper-Ramsey interrogation scheme, which effectively cancels field shifts and their related uncertainties [36, 37]. This method has been shown to suppress probe shifts by factors up to 2×10^3 [38] and even 10^4 [39]. Once in place, it will become possible to fully exploit the advantages of bosonic isotopes of Hg: a sensitivity to blackbody radiation 30 and 16 times smaller than Sr and Yb respectively, associated to an unlimited $^3\text{P}_0$ state lifetime to take the full benefit of best present and future ultrastable lasers. Highly accurate frequency ratio measurements involving Hg can contribute to validating optical clocks in view of a redefinition of the second [40] and to fundamental physics tests relying on diverse optical transitions [41–43].

Acknowledgments: Within the french national metrology network coordinated by LNE, LNE-OP at LTE-Observatoire de Paris is the national metrology institute for time, frequency and gravimetry. We acknowledge contributions of LTE electronic, mechanic and IT support services. C.Zyskind received funding from Sorbonne Université (PhD grant CMA FQPS n°ANR-21-CMAQ-0001 dans le cadre de France 2030).

-
- [1] S. Häfner, S. Falke, C. Grebing, S. Vogt, T. Legero, M. Merimaa, C. Lisdat, and U. Sterr, 8×10^{-17} fractional laser frequency instability with a long room-temperature cavity, *Opt. Lett.* **40**, 2112 (2015).
- [2] D. G. Matei, T. Legero, S. Häfner, C. Grebing, R. Weyrich, W. Zhang, L. Sonderhouse, J. M. Robinson, J. Ye, F. Riehle, and U. Sterr, 1.5 μm lasers with sub-10 mhz linewidth, *Phys. Rev. Lett.* **118**, 263202 (2017).
- [3] L. Yan, S. Lannig, W. R. Milner, M. N. Frankel, B. Lewis, D. Lee, K. Kim, and J. Ye, High-Power Clock Laser Spectrally Tailored for High-Fidelity Quantum State Engineering, *Phys. Rev. X* **15**, 031055 (2025).
- [4] H. Hachisu, K. Miyagishi, S. G. Porsev, A. Derevianko, V. D. Ovsiannikov, V. G. Pal'chikov, M. Takamoto, and H. Katori, Trapping of neutral mercury atoms and prospects for optical lattice clocks, *Phys. Rev. Lett.* **100**, 053001 (2008).
- [5] M. Petersen, R. Chicireanu, S. T. Dawkins, D. V. Magalhães, C. Mandache, Y. L. Coq, A. Clairon, and S. Bize, Doppler-free spectroscopy of the $^1\text{S}_0$ - $^3\text{P}_0$ optical clock transition in laser-cooled fermionic isotopes of neutral mercury, *Phys. Rev. Lett.* **101**, 183004 (2008).
- [6] K. Yamanaka, N. Ohmae, I. Ushijima, M. Takamoto, and H. Katori, Frequency ratio of ^{199}Hg and ^{87}Sr optical lattice clocks beyond the si limit, *Phys. Rev. Lett.* **114**, 230801 (2015).
- [7] R. Tyumenev, M. Favier, S. Bilicki, E. Bookjans, R. Le Targat, J. Lodewyck, D. Nicolodi, Y. Le Coq, M. Abgrall, J. Guéna, L. De Sarlo, and S. Bize, Comparing a mercury optical lattice clock with microwave and optical frequency standards, *New J. Phys.* **18**, 113002 (2016).
- [8] S. G. Porsev, U. I. Safronova, and M. S. Safronova, Theoretical study of the g factor and lifetime of the $6s6p\ ^3p_0$ state of mercury, *Phys. Rev. A* **96**, 012509 (2017).
- [9] M. C. Bignon, Probabilité de transition de la raie $6^1\text{S}_0 - 6^3\text{P}_0$ du mercure, *J. Phys. France* **28**, 51 (1967).
- [10] A. Al-Masoudi, S. Dörscher, S. Häfner, U. Sterr, and C. Lisdat, Noise and instability of an optical lattice clock, *Phys. Rev. A* **92**, 063814 (2015).
- [11] E. Oelker, R. B. Hutson, C. J. Kennedy, L. Sonderhouse, T. Bothwell, A. Goban, D. Kedar, C. Sanner, J. M. Robinson, G. E. Marti, D. G. Matei, T. Legero, M. Giunta, R. Holzwarth, F. Riehle, U. Sterr, and J. Ye, Demonstration of 4.8×10^{-17} stability at 1 s for two independent optical clocks, *Nature Photonics* **13**, 714 (2019).
- [12] N. Hinkley, J. A. Sherman, N. B. Phillips, M. Schioppa, N. D. Lemke, K. Beloy, M. Pizzocaro, C. W. Oates, and A. D. Ludlow, An atomic clock with 10^{-18} instability, *Science* **341**, 1215 (2013).
- [13] A. V. Taichenachev, V. I. Yudin, C. W. Oates, C. W. Hoyt, Z. W. Barber, and L. Hollberg, Magnetic field-induced spectroscopy of forbidden optical transitions with application to lattice-based optical atomic clocks, *Phys. Rev. Lett.* **96**, 083001 (2006).
- [14] X. Baillard, M. Fouché, R. L. Targat, P. G. Westergaard, A. Lecallier, Y. L. Coq, G. D. Rovera, S. Bize, and P. Lemonde, Accuracy evaluation of an optical lattice clock with bosonic atoms, *Opt. Lett.* **32**, 1812 (2007).
- [15] T. Takano, R. Mizushima, and H. Katori, Precise determination of the isotope shift of $^{88}\text{Sr} - ^{87}\text{Sr}$ optical lattice clock by sharing perturbations, *Appl. Phys. Express* **10**, 042401 (2017).

- 072801 (2017).
- [16] S. Origlia, M. S. Pramod, S. Schiller, Y. Singh, K. Bongs, R. Schwarz, A. Al-Masoudi, S. Dörscher, S. Herbers, S. Häfner, U. Sterr, and C. Lisdat, Towards an optical clock for space: Compact, high-performance optical lattice clock based on bosonic atoms, *Phys. Rev. A* **98**, 053443 (2018).
- [17] Z. W. Barber, C. W. Hoyt, C. W. Oates, L. Hollberg, A. V. Taichenachev, and V. I. Yudin, Direct excitation of the forbidden clock transition in neutral ^{174}Yb atoms confined to an optical lattice, *Phys. Rev. Lett.* **96**, 083002 (2006).
- [18] J. Millo, D. V. Magalhães, C. Mandache, Y. Le Coq, E. M. L. English, P. G. Westergaard, J. Lodewyck, S. Bize, P. Lemonde, and G. Santarelli, Ultrastable lasers based on vibration insensitive cavities, *Phys. Rev. A* **79**, 053829 (2009).
- [19] S. Dawkins, R. Chicreanu, M. Petersen, J. Millo, D. Magalhães, C. Mandache, Y. Le Coq, and S. Bize, An ultra-stable referenced interrogation system in the deep ultraviolet for a mercury optical lattice clock, *Appl. Phys. B: Lasers and Optics* **99**, 41 (2010).
- [20] S. Mejri, J. J. McFerran, L. Yi, Y. Le Coq, and S. Bize, Ultraviolet laser spectroscopy of neutral mercury in a one-dimensional optical lattice, *Phys. Rev. A* **84**, 032507 (2011).
- [21] J. J. McFerran, L. Yi, S. Mejri, W. Zhang, S. Di Manno, M. Abgrall, J. Guéna, Y. Le Coq, and S. Bize, Statistical uncertainty of 2.5×10^{-16} for the $^{199}\text{Hg } ^1S_0 - ^3P_0$ clock transition against a primary frequency standard, *Phys. Rev. A* **89**, 043432 (2014).
- [22] C. Guo, V. Cambier, J. Calvert, M. Favier, M. Andia, L. de Sarlo, and S. Bize, Exploiting the two-dimensional magneto-optical trapping of ^{199}Hg for a mercury optical lattice clock, *Phys. Rev. A* **107**, 033116 (2023).
- [23] C. Zyskind, *An optical lattice clock with a bosonic isotope of mercury*, Ph.D. thesis (2024), thèse de doctorat dirigée par Bize, Sébastien Physique Sorbonne université 2024.
- [24] J. J. McFerran, D. V. Magalhães, C. Mandache, J. Millo, W. Zhang, Y. Le Coq, G. Santarelli, and S. Bize, Laser locking to the $^{199}\text{Hg } ^1S_0 - ^3P_0$ clock transition with $5.4 \times 10^{-15}/\sqrt{\tau}$ fractional frequency instability, *Opt. Lett.* **37**, 3477 (2012).
- [25] Journal of research of the national institute of standards and technology, *J. Res. Natl. Inst. Stand. Technol.* **116**, 599 (2011), published online 2011 Apr 1.
- [26] Journal of physical and chemical reference data, *J. Phys. Chem. Ref. Data* **35**, 1519 (2006).
- [27] H. Katori, M. Takamoto, V. G. Pal'chikov, and V. D. Ovsiannikov, Ultrastable optical clock with neutral atoms in an engineered light shift trap, *Phys. Rev. Lett.* **91**, 173005 (2003).
- [28] The additional uncorrelated frequency noise was estimated to be 0.61 Hz, corresponding to the value required to bring the goodness of fit to the nominal value of 0.5, or equivalently, the Birge ratio to 1.
- [29] The QSZ coefficient is extracted from series of measurements with optimal pulses at several currents and several probe powers. A fit to these measurements is used to obtain both the QSZ coefficient and the probe light shift coefficient.
- [30] C. Guo, M. Favier, N. Galland, V. Cambier, H. Álvarez Martínez, M. Lours, L. De Sarlo, M. Andia, R. Le Targat, and S. Bize, Accurate laser frequency locking to optical frequency combs under low-signal-to-noise-ratio conditions, *Rev. Sci. Instrum.* **91**, 033202 (2020).
- [31] J. Lodewyck, S. Bilicki, E. Bookjans, J.-L. Robyr, C. Shi, G. Vallet, R. Le Targat, D. Nicolodi, Y. Le Coq, J. Guéna, M. Abgrall, P. Rosenbusch, and S. Bize, Optical to microwave clock frequency ratios with a nearly continuous strontium optical lattice clock, *Metrologia* **53**, 1123 (2016).
- [32] Sr clocks used in this work are LTE clocks. They are identified by the BIPM as SYRTE-Sr2 and SYRTE-SrB until the end of 2024, and LNEOP-Sr2 and LNEOP-SrB since January 1st 2025.
- [33] K. Gibble, Scattering of cold-atom coherences by hot atoms: Frequency shifts from background-gas collisions, *Phys. Rev. Lett.* **110**, 180802 (2013).
- [34] M. Abdel-Hafiz, P. Ablewski, A. Al-Masoudi, H. Álvarez Martínez, P. Balling, G. Barwood, E. Benkler, M. Bober, M. Borkowski, W. Bowden, R. Ciuryło, H. Cybulski, A. Didier, M. Doležal, S. Dörscher, S. Falke, R. M. Godun, R. Hamid, I. R. Hill, R. Hobson, N. Huntemann, Y. L. Coq, R. L. Targat, T. Legero, T. Lindvall, C. Lisdat, J. Lodewyck, H. S. Margolis, T. E. Mehlstäubler, E. Peik, L. Pelzer, M. Pizzocaro, B. Rauf, A. Rolland, N. Scharnhorst, M. Schioppo, P. O. Schmidt, R. Schwarz, Çağrı Şenel, N. Spethmann, U. Sterr, C. Tamm, J. W. Thomsen, A. Vianello, and M. Zawada, *Guidelines for developing optical clocks with 10^{-18} fractional frequency uncertainty* (2019), arXiv:1906.11495 [physics.atom-ph].
- [35] H. S. Margolis, G. Panfilo, G. Petit, C. Oates, T. Ido, and S. Bize, The CIPM list 'Recommended values of standard frequencies': 2021 update, *Metrologia* **61**, 035005 (2024).
- [36] V. I. Yudin, A. V. Taichenachev, C. W. Oates, Z. W. Barber, N. D. Lemke, A. D. Ludlow, U. Sterr, C. Lisdat, and F. Riehle, Hyper-Ramsey spectroscopy of optical clock transitions, *Phys. Rev. A* **82**, 011804 (2010).
- [37] T. Zanon-Willette, R. Lefevre, R. Metzдорff, N. Sillitoe, S. Almonacil, M. Minissale, E. de Clercq, A. V. Taichenachev, V. I. Yudin, and E. Arimondo, Composite laser-pulses spectroscopy for high-accuracy optical clocks: a review of recent progress and perspectives, *Reports on Progress in Physics* **81**, 094401 (2018).
- [38] R. Hobson, W. Bowden, S. King, P. Baird, I. Hill, and P. Gill, Modified hyper-ramsey methods for the elimination of probe shifts in optical clocks, *Physical Review A* **93** (2015).
- [39] N. Huntemann, B. Lipphardt, M. Okhapkin, C. Tamm, E. Peik, A. V. Taichenachev, and V. I. Yudin, Generalized ramsey excitation scheme with suppressed light shift, *Phys. Rev. Lett.* **109**, 213002 (2012).
- [40] N. Dimarcq, M. Gertsvolf, G. Mileti, S. Bize, C. W. Oates, E. Peik, D. Calonico, T. Ido, P. Tavella, F. Meynadier, G. Petit, G. Panfilo, J. Bartholomew, P. Defraigne, E. A. Donley, P. O. Hedekvist, I. Sesia, M. Wouters, P. Dubé, F. Fang, F. Levi, J. Lodewyck, H. S. Margolis, D. Newell, S. Slyusarev, S. Weyers, J.-P. Uzan, M. Yasuda, D.-H. Yu, C. Rieck, H. Schnatz, Y. Hanado, M. Fujieda, P.-E. Pottie, J. Hanssen, A. Malimon, and N. Ashby, Roadmap towards the redefinition of the second, *Metrologia* **61**, 012001 (2024).
- [41] B. M. Roberts, P. Delva, A. Al-Masoudi, A. Amy-Klein, C. Bærentsen, C. F. A. Baynham, E. Benkler, S. Bilicki, S. Bize, W. Bowden, J. Calvert, V. Cambier, E. Cantin, E. A. Curtis, S. Dörscher, M. Favier, F. Frank, P. Gill,

- R. M. Godun, G. Grosche, C. Guo, A. Hees, I. R. Hill, R. Hobson, N. Huntemann, J. Kronjäger, S. Koke, A. Kuhl, R. Lange, T. Legero, B. Lipphardt, C. Lisdat, J. Lodewyck, O. Lopez, H. S. Margolis, H. Álvarez-Martínez, F. Meynadier, F. Ozimek, E. Peik, P.-E. Pottie, N. Quintin, C. Sanner, L. D. Sarlo, M. Schioppo, R. Schwarz, A. Silva, U. Sterr, C. Tamm, R. L. Targat, P. Tuckey, G. Vallet, T. Waterholter, D. Xu, and P. Wolf, Search for transient variations of the fine structure constant and dark matter using fiber-linked optical atomic clocks, [New J. Phys.](#) **22**, 093010 (2020).
- [42] M. S. Safronova, D. Budker, D. DeMille, D. F. J. Kimball, A. Derevianko, and C. W. Clark, Search for new physics with atoms and molecules, [Rev. Mod. Phys.](#) **90**, 025008 (2018).
- [43] J.-P. Uzan, Fundamental constants: From measurement to the universe, a window on gravitation and cosmology, [Living Rev Relativ](#) **28**, 6 (2025).